Title

Can the salt-advection feedback be detected in internal variability of the Atlantic Meridional Overturning Circulation? Can the salt-advection feedback be detected in internal variability of the Atlantic Meridional Overturning Circulation?

Journal

Journal of Climate, 31(16)

ISSN

0894-8755

Authors

Cheng, Wei

Weijer, Wilbert

Kim, Who M

et al.

Publication Date

2018

DOI

10.1175/jcli-d-17-0825.1

Peer reviewed

Can the Salt-Advection Feedback Be Detected in Internal Variability of the Atlantic Meridional Overturning Circulation?

WEI CHENG, a,b

WILBERT WEIJER, c

WHO M. KIM, d

GOKHAN DANABASOGLU, d

STEVE G. YEAGER, d

PETER R. GENT, d

DONGXIAO ZHANG, a,b

JOHN C. H. CHIANG, e

AND JIAXU ZHANGc

a Joint Institute for the Study of Atmosphere and Ocean, University of Washington, Seattle, Washington

b Pacific Marine Environmental Laboratory, NOAA, Seattle, Washington

c Los Alamos National Laboratory, Los Alamos, New Mexico

d National Center for Atmospheric Research, Boulder, Colorado

e University of California, Berkeley, Berkeley, California

ABSTRACT

Evidence for the assumptions of the salt-advection feedback in box models is sought by studying the Atlantic meridional overturning circulation (AMOC) internal variability in the long preindustrial control runs of two Earth system models. The first assumption is that AMOC strength is proportional to the meridional density difference between the North Atlantic and the Southern Oceans. The model simulations support this assumption, with the caveat that nearly all the long time-scale variability occurs in the North Atlantic density. The second assumption is that the freshwater transport variability by the overturning at the Atlantic southern boundary is controlled by the strength of AMOC. Only one of the models shows some evidence that AMOC variability at 45°N leads variability in the overturning freshwater transport at the southern boundary by about 30 years, but the other model shows no such coherence. In contrast, in both models this freshwater transport variability is dominated by local salinity variations. The third assumption is that changes in the overturning freshwater transport at the Atlantic southern boundary perturb the north–south density difference, and thus feed back on AMOC strength in the north. No evidence for this assumption is found in either model at any time scale, although this does not rule out that the salt-advection feedback may be excited by a strong enough freshwater perturbation.

1. Introduction

Thresholds in the climate system could lead to rapid change, even if trends in climate forcing are weak. One such threshold is related to the possibility that the Atlantic meridional overturning circulation (AMOC) has two stable equilibrium states under the same forcing conditions: namely, our current state with a strong overturning circulation, northward heat transport in the Atlantic, and deep-water formation in the subpolar North Atlantic; and a state with collapsed AMOC. If the current climate state would indeed allow for a permanent collapse of AMOC, then finite amplitude disturbances, such as abrupt meltwater input from the Greenland ice sheet, or slight but permanent changes in external forcing, such as changes in the hydrological cycle, could potentially trigger a transition to the off state, with severe implications for the climate system.

Stommel (1961) was the first to postulate that thermohaline flows could have multiple equilibrium states for a given forcing condition. He studied the dynamics of density-driven overturning circulation using a simple two-box model, one representing a warm and salty box, the other representing a cold and fresh box. He showed the crucial importance of a positive feedback between overturning strength and advection of salt into the ‘‘cold’’ box, the salt-advection feedback. This feedback links the overturning strength to the meridional density difference; while in turn this density difference is controlled by the meridional advection of salt by the overturning. The Stommel box model was later expanded by others to allow for interhemispheric flow. In particular, Rahmstorf (1996) built on Rooth’s (1982) three-box model to show that the salt-advection feedback can also lead to multiple equilibria of interhemispheric flow. One main finding of Rahmstorf (1996) is that AMOC stability depends on the sign of AMOC-driven freshwater flux across the southern boundary of the Atlantic at 34°S, hereafter referred to as Fov. When Fov is positive, a stronger AMOC transports more freshwater into the Atlantic Ocean, thus weakening AMOC; in this case, the salt-advection feedback is negative and has a stabilizing effect. Conversely, when Fov is negative, a stronger AMOC transports more freshwater out of the Atlantic, thus strengthening AMOC; in this case, the salt-advection feedback is positive and has a destabilizing tendency.

Studies with more comprehensive models suggest that the sign of Fov is a predictor of the existence of the off state (de Vries and Weber 2005); that is, the sign of Fov determines if AMOC is in a bistable or monostable regime. Later studies have refined this metric; in particular by including AMOC-related freshwater transport at the northern basin boundary as well (Dijkstra 2007; Huisman et al. 2010; Liu and Liu 2013, 2014). Nevertheless, the accuracy of Fov as a stability indicator depends on the relative importance of Fov as compared to other freshwater transport processes for maintaining the Atlantic Ocean freshwater budget (e.g., Sijp et al. 2012; Cimatoribus et al. 2014). In particular, it is well known that the Atlantic basin from 34°S to 65°N is net evaporative (Wijffels et al. 1992), so for a quasi-steady ocean state, this surface freshwater loss needs to be balanced by the sum of freshwater transports by the overturning, wind-driven gyres, and eddy-driven mixing across its northern and southern boundaries. But despite this evaporative freshwater loss, observational analysis suggests that the overturning actually becomes fresher while

traversing the Atlantic, as the southward branch of AMOC is fresher than the northward branch at 34°S (e.g., Weijer et al. 1999); this leaves the gyre circulation to compensate for both net evaporation and freshwater export by AMOC. Freshwater transport by the gyre and overturning circulations at a given latitude depends on the spatial correlations of salinity and velocity fields at that latitude; specifically, the direction and amplitude of Fov depends on whether the northward branch of AMOC is located primarily in the high-salinity surface layer or the relatively fresh intermediate layer (Gordon 1986). Therefore, even though the total freshwater transport by these processes is known a priori, there are no obvious external constraints on the partitioning between the components.

This partitioning is important for discussion of the role of Fov as a stability indicator, as this paradigm assumes that Fov satisfies an externally imposed constraint on both the active AMOC and a potentially collapsed state. In box models, where only the overturning circulation transports freshwater, this constraint is net evaporation from the basin. But several modeling studies with more comprehensive models show that the stability characteristics of AMOC can also be changed by artificially changing gyre-induced freshwater transport across 34°S in the South Atlantic, hence forcing Fov to satisfy both net evaporation and gyre-induced transport (de Vries and Weber 2005; Cimatoribus et al. 2012; Jackson 2013). In fully coupled climate models, however, no constraints exist in either the net surface freshwater flux or total oceanic meridional freshwater transport, and the gyreinduced freshwater flux can differ significantly between active and collapsed AMOC states. This was demonstrated by Mecking et al. (2016), who induced an AMOC collapse in an eddy-permitting climate model through a traditional ‘‘hosing’’ approach, and showed that the difference in gyre-driven freshwater transport between an active and a collapsed AMOC state is larger than the difference in Fov. Their Fov is negative in both the active and collapsed AMOC states, and the model maintains a collapsed state for 450 years. The authors suggest that AMOC is bistable in the model, although it can be argued that maintaining a collapsed state for 450 yr is not conclusive proof that this state is truly a stable equilibrium (see, e.g., Gent 2018).

Regardless of the partitioning between freshwater transport components, the salt-advection feedback mechanism depends critically on several assumptions. The first is that AMOC strength is proportional to the meridional density difference between the North Atlantic and Southern Ocean. This buoyancy-driven relationship is supported by general circulation modeling studies (e.g., Griesel and Maqueda 2006), and found to explain over 75% of AMOC variability in both the upper ocean (at 1000m) and at depth (4000 m) on multidecadal and longer time scales (Butler et al. 2016). However, its theoretical underpinning is called into question (e.g., de Boer et al. 2010), particularly in light of the role of Southern Ocean winds in forcing the AMOC upwelling branch and setting up global ocean stratification, and the adiabatic nature of interior ocean circulation (Toggweiler and Samuels 1998; Gnanadesikan 1999). Nonetheless, even studies that account for these complexities tend to uncover the salt-advection feedback as a source of multiple equilibria (Johnson et al. 2007; Cimatoribus et al. 2014; Wolfe and Cessi 2014, 2015).

The second implicit assumption is that Fov is primarily controlled by ocean meridional velocity rather than the salinity distribution at that latitude. In Rahmstorf's (1996) box model, the AMOC-driven freshwater transport depends on both the salinity difference between the northern and southernmost boxes and the strength of AMOC transport [his Eq. (1)]; in particular, an increase in AMOC strength would necessarily be balanced by a decrease in salinity difference given a fixed atmospheric transport. In reality, as mentioned above, several mechanisms are responsible for closing the basin salinity– freshwater balance, and both AMOC strength and salinity difference may change independently in the equilibration process. For example, based on the intermodel spread of the time-mean states, Mecking et al. (2017) find a correlation between Fov and AMOC in a large number of equilibrated coupled model simulations, but conclude that this correlation is due to the dependence of the salinity biases on AMOC, rather than on AMOC itself. In other words, models with a stronger AMOC also feature an enhanced salinity stratification at 34°S, and this term [the ''S2–S1'' from Rahmstorf's (1996) Eq. (1)] dominates Fov, not the transport associated with AMOC itself [the ''m'' in Rahmstorf's (1996) Eq. (1)].

The third assumption is that changes in Fov perturb the north–south density difference, and as such, they feed back on AMOC. However, it is not clear what amplitude and duration of perturbations in Fov are required to have a sufficient impact on the density in the North Atlantic to significantly affect AMOC strength. Several studies have addressed the northward propagation of salinity anomalies in the Atlantic and their dynamical impact, mostly in the context of Agulhas leakage. Weijer et al. (2002), for instance, implemented a salt source in the South Atlantic of a low-resolution ocean model to mimic the salt released by Agulhas rings on their passage westward across the basin. In a quasisteady experiment in which the salt source was gradually increased on millennial time scales, AMOC response was found to be almost linearly related to the source strength. However, Weijer and van Sebille (2014) studied internal variability in a fully coupled climate system model, and did not find a significant impact of Agulhas leakage salt fluxes on AMOC, despite the fact that salinity anomalies were found to reach the North Atlantic. These studies suggest that the amplitude and time scale of salt flux variability matter in some ways for their impact on AMOC.

So far, studies addressing the salt-advection feedback and AMOC stability in general circulation models apply a strong instantaneous salinity perturbation or strong transient surface freshwater flux perturbation to the North Atlantic (freshwater hosing), and examine how AMOC behaves during and after the hosing and its relationships with Fov (e.g., Huisman et al. 2010; Jackson 2013; Liu et al. 2014; den Toom et al. 2014; Mecking et al. 2016). These studies find that AMOC recovers later and/or at a slower rate when the equilibrium-state Fov (before hosing) is negative, and vice versa. Nonetheless, these studies leave several issues unanswered. First, the large amplitude of the freshwater perturbations, and the strong responses they generate, lead to strong nonlinearities in the system evolution that often make it difficult to separate the impacts of velocity and salinity perturbations individually. Second, the instantaneous application of these perturbations does not allow for a

careful examination of the time scales on which different elements of the saltadvection feedback are active, or most effective. This is relevant, since many studies that attempt to interpret AMOC behavior in terms of Fov are considering transient future warming scenarios (e.g., Weaver et al. 2012). Third, the dedicated hosing experiments are expensive, making a systematic comparison of the robustness of the elements of the salt-advection feedback among a suite of models very unlikely.

Here we take a different approach: we seek evidence for the different assumptions of the salt- advection feedback by studying internal variability of AMOC on decadal and longer time scales. In particular, we will use spectral analysis on key metrics of AMOC variability from two centennial-scale climate simulations to understand the relationship between AMOC strength and Fov, the processes involved, and the time scales on which they operate. Based on analysis of internal AMOC variability alone, however, we will not be able to draw definitive conclusions regarding AMOC bistability in these models. Nonetheless, we work off the assumption that the salt-advection feedback not only helps to shape the equilibrium structure of AMOC, but also the temporal evolution of perturbations around these equilibria (e.g., Stommel 1961). In other words, the feedback that can lead to multiple equilibria is the same as the process that can trigger a transition between those equilibria. That said, many other feedbacks exist, both in the real world and in reduced models, which keep AMOC stable to small-amplitude perturbations, so we are seeking signatures of a particular, potentially destabilizing feedback amidst a host of other feedbacks that keep AMOC stable.

To set the stage, we first examine basinwide (from 34°S to 65°N) mean-state freshwater transport by AMOC, called Fov(y), in the preindustrial control simulations of two Earth system models (ESMs). Our results are similar to those of Mecking et al. (2017) in that we find that the salinity bias in these ESM simulations causes a positive bias in modeled Fov in the South Atlantic. We then decompose Fov(y) decadal and longer time-scale variability in these runs into contributions from the salinity and meridional velocity anomalies, and covariability of salinity and velocity anomalies or the eddy component, and compare the magnitudes of the components and investigate how each component varies with latitude. Last, using Fov(y) and the AMOC index throughout the basin, we examine the relationship between AMOC and meridional density difference, and the North Atlantic versus Southern Ocean's contribution to the density difference; and the relationship between Fov(y) and AMOC variability, with a particular focus on meridional coherence and propagation properties of the signal. These analyses are aimed at examining the key assumptions underlying the basin-scale (from the Southern Ocean to the subpolar North Atlantic) salt-advection feedback mechanism described above.

The rest of the paper is organized as follows. In section 2, we briefly describe the ESMs used in this study and introduce specific metrics, observational data, and statistical methods. The main results are presented in section 3, and section 4 discusses the broader implications of our results and remaining challenges. Section 5 contains the conclusions.

2. Methods

To examine the salt-advection feedback associated with internal variability of AMOC, we use preindustrial control simulations from the Geophysical Fluid Dynamics Laboratory (GFDL)-ESM2M and the National Center for Atmospheric Research (NCAR) CESM1— two leading ESMs. The external climate forcings (greenhouse gas emissions, volcanic and anthropogenic aerosols, solar irradiance) in these simulations are held constant at their preindustrial levels, which is usually taken as the conditions in year 1850. Detailed descriptions of these models and their 1850 control runs are presented in Dunne et al. (2012) and Kay et al. (2015), respectively, and references therein. Briefly, the horizontal resolution of the ocean and sea ice components in both models is nominally 18; CESM1 has 60 vertical levels in the ocean while ESM2M has 50. The sea ice components use the same horizontal grid as the respective ocean components. The atmosphere and land components have a horizontal resolution of 28 in ESM2M and 18 in CESM1. For ESM2M, a 500-yr control simulation after the initial spinup is available through the GFDL data portal. For CESM1 quasi-equilibrium state, we use years 800–2200 from the long 1850 control simulation. Monthly mean ocean potential temperature (T), salinity (S), and velocity fields from these simulations are used in our analysis.

We employ an AMOC index computed as the maximum value of the annual-mean overturning streamfunction in depth–latitude space below 500 m. This index is computed for each latitude from 34°S to 65°N, the expansion of the ocean basin with landmass on either side. Between 45° and 60°N, the mean value of the AMOC index and its interannual variability depends on whether it is defined on density or depth space (Zhang 2010). Nonetheless, the two indices are strongly correlated from the South Atlantic to roughly 50°N, and in intermittent bands north of 50°N (not shown). Our statistical analysis will use the AMOC index at 45°N, and therefore the results would not depend on whether the AMOC index is defined in density or depth space. Following Drijfhout et al. (2011), Fov and its expansion to other latitudes of the Atlantic Ocean between 34°S and 65°N, namely, Fov(y), is computed as

$$\mathrm{Fov}(y) = \frac{-1}{\mathrm{So}} \sum_{\mathrm{bot}}^{\mathrm{sfc}} \{V^*\}(y,z)\langle S\rangle(y,z), \qquad (1)$$

where So is the reference salinity equal to 35 psu, V* is the baroclinic meridional velocity with section mean removed and braces indicating its across-basin zonal integral, S is salinity with ‹·› denoting its across-basin zonal average, and $\sum_{bot}^{sfc}$ bot represents the vertical integral from the sea surface to the ocean bottom. The contributions from the bottom water (delineated by regions below 4 km with northward baroclinic meridional velocity) to the full-depth-integrated Fov in these models are insignificant, a result that is consistent with Drijfhout et al. (2011); therefore, we did not exclude the bottom water contribution (i.e., the Southern Ocean branch of AMOC) in our final calculations of Fov. Variables {V*} and ‹S› are computed as functions of latitude (y) and ocean depth (z). Because the vertical integral of V* is zero, values of Fov(y) are unchanged if a constant reference salinity

is added or removed from ‹*S*› in the above equation. Variables {V*}(*x*, *y*), ‹*S*›(*x*, *z*), and Fov(*y*) are calculated using the monthly mean model output, and the derived monthly fields are averaged over each year to form annual-mean time series.

Temporal variability in the annual-mean time series of Fov(*y*) is decomposed into contributions from meridional velocity and salinity, respectively, using the following equation; we simplify the symbols {V*} to y, and ‹*S*›/So to *s*, noting these terms are functions of latitude:

$$\begin{aligned} \mathrm{Fov}(y) &= \sum_{\mathrm{bot}}^{\mathrm{sfc}} v \times s = \sum_{\mathrm{bot}}^{\mathrm{sfc}} (\overline{v} + v')(\overline{s} + s') \\ &= \sum_{\mathrm{bot}}^{\mathrm{sfc}} (\overline{v}\,\overline{s} + \overline{v}s' + v'\overline{s} + v's') \end{aligned} \qquad (2.1)$$

Or

$$\mathrm{Fov}(y) - \sum_{\mathrm{bot}}^{\mathrm{sfc}} \overline{v}\,\overline{s} = \mathrm{Fov}'(y) = \sum_{\mathrm{bot}}^{\mathrm{sfc}} (\overline{v}s' + v'\overline{s} + v's'), \qquad (2.2)$$

(a) (b) (c)

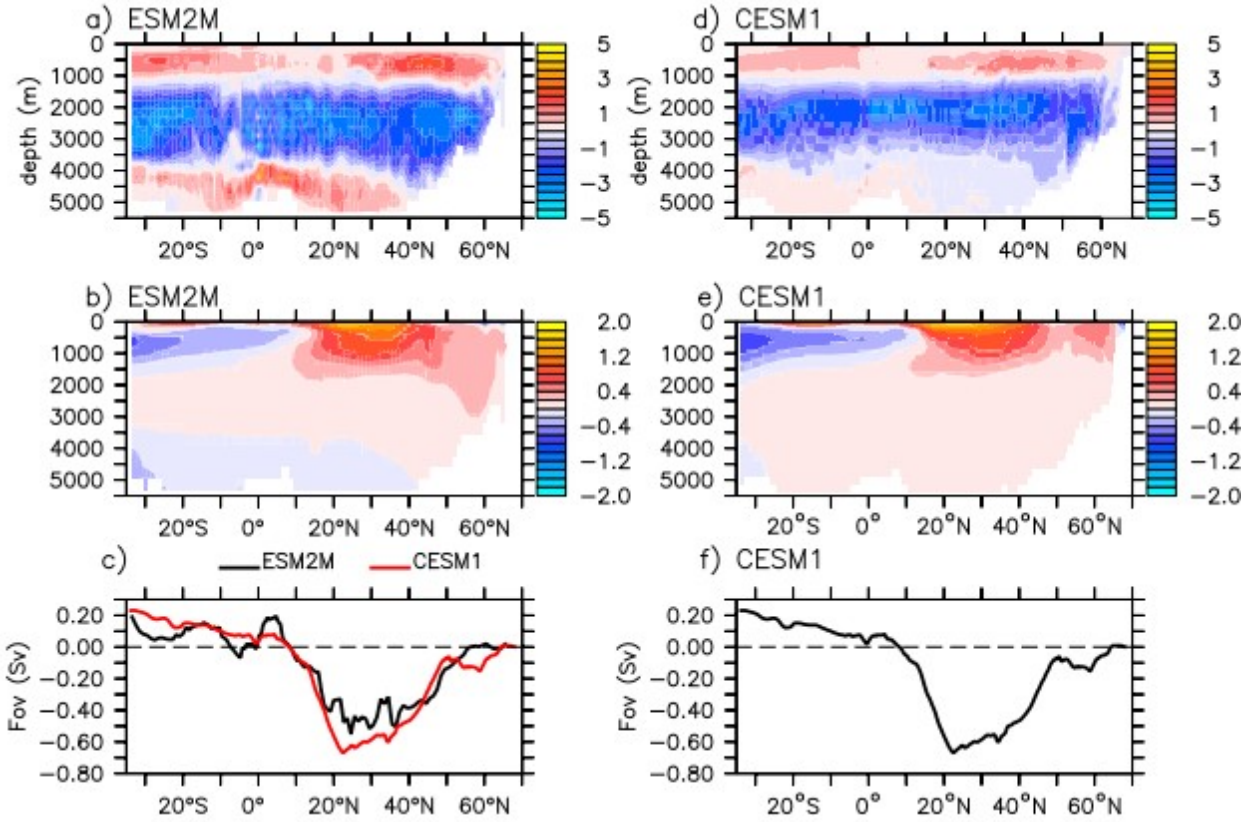

FIG. 1. Long-term mean Atlantic Ocean zonally integrated baroclinic meridional velocity $[\mathrm{Sv}\ (1\ \mathrm{Sv} \equiv 10^6\ \mathrm{m^3\ s^{-1}})]$ in (a) ESM2M and (d) CESM1. Zonally averaged salinity minus 35 (psu) in (b) ESM2M and (e) CESM1. Freshwater transport by AMOC at each latitude, Fov(y) (Sv), in (c) ESM2M and (f) CESM1. The CESM1 result is redrawn in (c) (red line). No meridional smoothing is applied.

Where $\sum_{bot}^{sfc}$ again represents the surface-to-bottom vertical integral as in Eq. (1), the overbar represents the long-term mean, and the 0 represents deviations from the long-term mean. The left-hand side of Eq. (2.2), Fov′ (y) is the Fov(y) anomaly with its long-term mean at each latitude removed; (a) and (b) on the right-hand side denote the contributions from salinity and velocity anomalies around their respective long-term means, and (c) denotes contributions from covariability between the salinity and velocity anomalies.

In addition to the model output, we also use monthly mean ocean potential temperature and salinity from the Hadley Centre EN4 dataset (http://www.metoffice.gov. uk/hadobs/en4/), which is quality-controlled ocean in situ observations objectively mapped onto a global 1° × 1° grid. The EN4 dataset is available from year 1901 to present.

Cross-correlation functions at both positive and negative lags, univariate spectrum, and cross-spectrum analyses are used to quantify relationships between the different variables. From the cross-spectrum analysis, we present coherence squared and coherence phase as a function of time period.

3. Results

a. Factors influencing Fov(y) mean state and temporal variability

We first quantify the quasi-equilibrium state of AMOC and Fov(y). The long-term mean (averaged over the entire 500 yr of ESM2M control simulation, and years 800–2200 of CESM1) zonally integrated baroclinic meridional velocities (Figs. 1a,d) show basinwide southward-moving North Atlantic Deep Water (NADW) sandwiched between the northward-moving thermocline (above 1 km) and bottom waters (below 3.5–4 km), characteristic of the interhemispheric flow pattern associated with AMOC. Quantitatively, the ESM2M meridional circulation is stronger than that of CESM1. Northward of 10°N, the long-term mean across-basin zonally averaged salinity decreases monotonically with depth below a fresh and shallow surface layer (Figs. 1b,e); this salinity vertical distribution, in combination with the direction of the overturning circulation (i.e., northward flow in the upper layer and southward flow in the lower layers), leads to positive meridional salt transport, or negative Fov(y), at these latitudes (Figs. 1c,f). South of 10°N, zonally averaged salinity has an intermediate-depth minimum associated with the Antarctic Intermediate Water (AAIW); as a result, Fov(y) switches sign to being positive. The meridional profiles of Fov(y) from the two models are similar despite the difference in their overturning strengths (Figs. 1a,d), and both are within the range of intermodel spread of the same metric across CMIP5 models (Mecking et al. 2017). In addition, the overturning circulation pattern does not appear to change much meridionally, while

Fov(y) changes significantly with latitude. These results suggest that the Fov(y) latitudinal structure in the ESMs is dictated by changes in the salinity distribution with latitude.

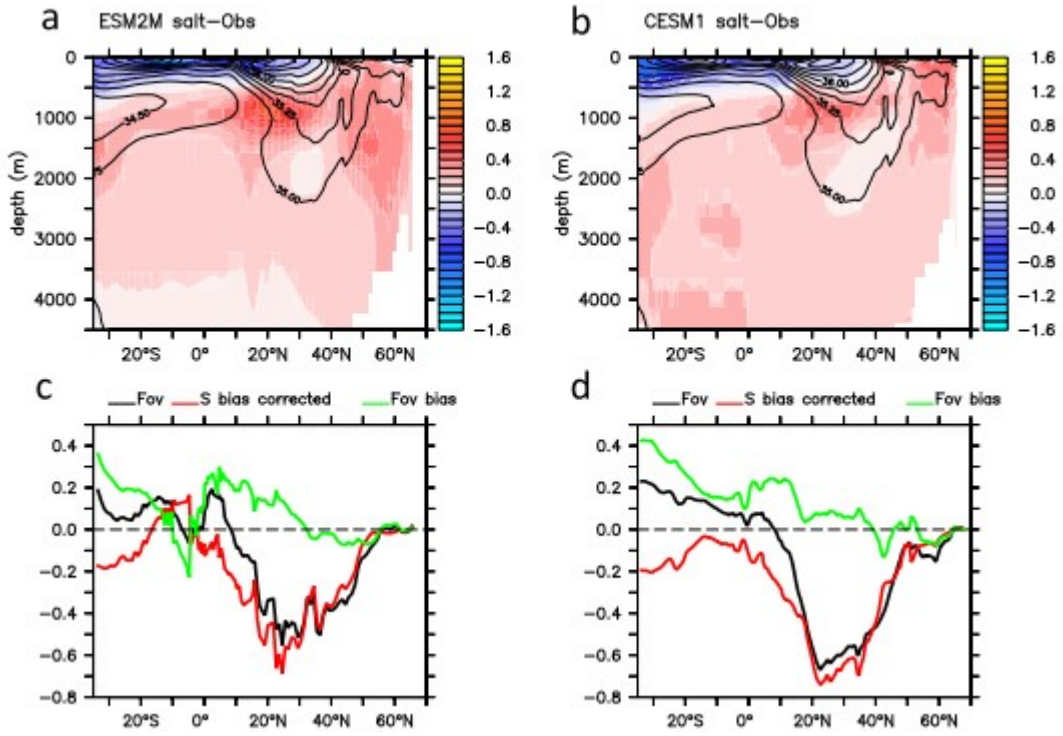

FIG. 2. Long-term mean Atlantic zonally averaged salinity bias (model 2 observation; psu; color shading) and observed zonally averaged salinity (psu; black contours) in (a) ESM2M and (b) CESM1. Long-term mean Fov(y) (black line), resulting Fov(y) when salinity bias is removed in computing Fov(y) (red line), and difference between original and salinity bias–corrected Fov(y) (green line) in (c) ESM2M and (d) CESM1. Units in (c) and (d): Sv.

However, both models have quite large salinity biases throughout the Atlantic, which is typical of most ESMs (e.g., Mecking et al. 2017). North of 40°N, the long-term mean zonally averaged salinity in ESM2M is too high in comparison to EN4 1901–20 (years in EN4 least affected by anthropogenic forcing, with the caveat that data coverage in earlier years is poorer than in later years) mean state except in a very thin layer near the sea surface where the model is too fresh (Fig. 2a). The salinity bias vertical gradient is quite weak north of roughly 40°N, but becomes stronger south of this latitude all the way to the South Atlantic, where the bias shows a dipole in the vertical direction with the water above (below) 800 m being too fresh (salty) (Fig. 2a). CESM1 shows a similar salinity bias to ESM2M, again with negative (positive) bias above (below) 800 m (Fig. 2b) south of 40°N. When the ESM2M zonally averaged salinity bias (Fig. 2a) is removed from hSi, the resulting Fov(y) (Fig. 2c, red line) south of 30°N shifts to more negative values compared to the Fov(y) without the salinity bias correction (Fig. 2c, black line). In particular, the salinitycorrected Fov(y) at the southern boundary of the Atlantic Ocean, namely,

Fov, is negative, whereas it is positive without the bias correction. In other words, if the model-simulated salinity had no bias, Fov would have been negative given the same simulated overturning circulation. The CESM1 results (Figs. 2b,d) are qualitatively similar to ESM2M, and both are consistent with the CMIP5 multimodel result presented in Fig. 3 of Mecking et al. (2017).

What layer(s) contribute to the positive Fov biases? In both ESMs, the salinity bias changes sign at about 800-m depth (Fig. 3, black lines), whereas the baroclinic meridional velocity changes sign from northward to southward flow at 1.2-km depth (Figs. 1a,d). These features combine to give rise to the positive Fov bias integrand (i.e., $V \times S_{bias}$ in each vertical layer) in both the upper ocean (above 800 m) and the NADW depths (1.2–4 km), as demonstrated by the red lines in Fig. 3. Similar dipoles in the vertical profiles of salinity bias occupy a wide range of the Atlantic Ocean from 34°S to roughly 30°N, resulting in positive bias in Fov(y) over those latitudes (Figs. 2c,d, green line).

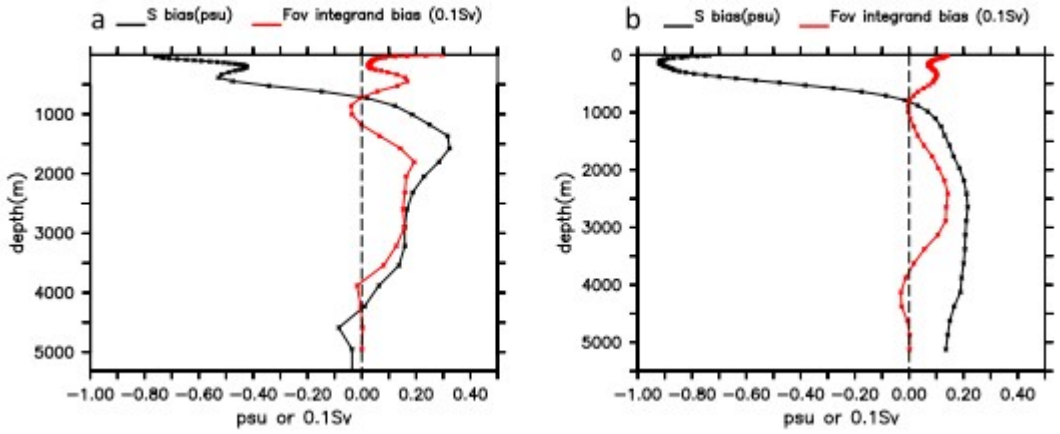

FIG. 3. Long-term mean vertical profile of the Atlantic zonally averaged salinity bias at 34°S (black line; psu) and the integrand of Fov bias due to the salinity bias (red line; Sv) in (a) ESM2M and (b) CESM1. The symbols in the plots indicate the midpoint of the vertical layers in the models.

To provide another perspective on the role of salinity biases on the sign of Fov, we consider the evolution of Fov and its components during the initial spinup phase of CESM1 (output during spinup is only available from CESM1). Using Eqs. (2.1) and (2.2), we obtain the relative contributions of salinity and meridional velocity on Fov temporal change. The CESM1 ocean component was initialized from the January-mean climatological Polar Science Center Hydrographic Climatology (PHC2) potential temperature and salinity data [the PHC2 dataset represents a blending of the Levitus et al. (1998) and Steele et al. (2001) data for the Arctic Ocean] and state of rest. As such, within a year from initialization, geostrophic adjustment renders the ocean circulation to be near its final quasi-equilibrium state (Fig. 4, green line) while the tracer fields undergo continuous but significant changes. Adjustment in the salinity causes total Fov to change from being negative in the initial condition to positive around year 80 (Fig. 4, black dashed line). After approximately year 140, the adjustment of Fov slows down but continues, again

mainly because of salinity adjustment (Fig. 4, red line). Contribution from covariability between the salinity and velocity anomalies is near zero after the first few decades (Fig. 4, cyan line).

Once reaching the quasi-equilibrium state, Fov(y) in both models exhibits natural variability on decadal and longer time scales. Again, following Eq. (2.2), we decompose the total variability of Fov (Fig. 5, black lines) into that due to salinity (Fig. 5, red lines) and velocity variations (Fig. 5, green lines). Although having a much smaller amplitude than those during the initial adjustment period, internal variability of Fov is similarly more correlated with local salinity variations than with local circulation changes. Specifically, in ESM2M (CESM1), the salinity anomaly accounts for 92% (57%) of the Fov variability while velocity anomaly accounts for 25% (35%) (Figs. 5a,b). The lower correlation in CESM1 between Fov and salinity variations is mostly caused by two periods in the late 900s and 1100s (Fig. 5b), when the Fov variability is dictated by changes in the meridional velocity. No such episodes occur in the ESM2M control run (Fig. 5a). Over the domain we considered (from 34°S to 65°N), the largest decadal variability in Fov(y) occurs between 15° and 45°N (Figs. 6a,b), and is dominantly caused by variability in the meridional velocity at these latitudes (Figs. 6e,f). North of 45°N and south of 15°N, Fov(y) anomalies are smaller and mostly caused by variability in the salinity field (Figs. 6c,d), with very small contributions from the region's velocity variations (Figs. 6e,f), consistent with Fig. 5.

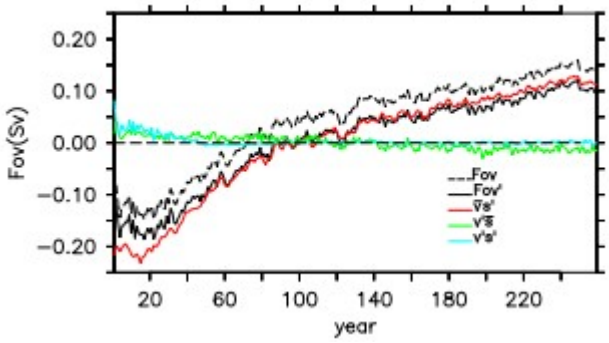

FIG. 4. Unfiltered annual-mean time series of Fov during the initial spinup of CESM1 (black dashed line); time series of Fov anomaly with the long-term mean of Fov over this time period removed (black solid line); contributions from salinity (red line) and velocity (green line) adjustment, and covariability between the salinity and velocity adjustments (cyan line) to Fov anomalies.

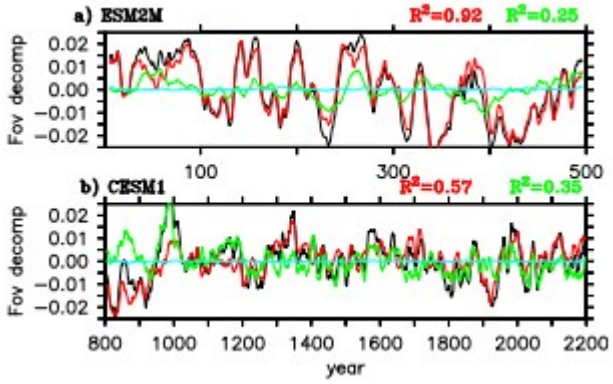

FIG. 5. Eleven-point running averages of the annual-mean time series of Fov anomalies (black lines; Sv) in (a) ESM2M and (b) CESM1, and its contributions from salinity (red line) and velocity (green line) variability, and covariability between salinity and velocity anomalies (cyan line). The R^2 values, computed using the shown time series, are color-coded to indicate if it is between the green or red time series with the black time series.

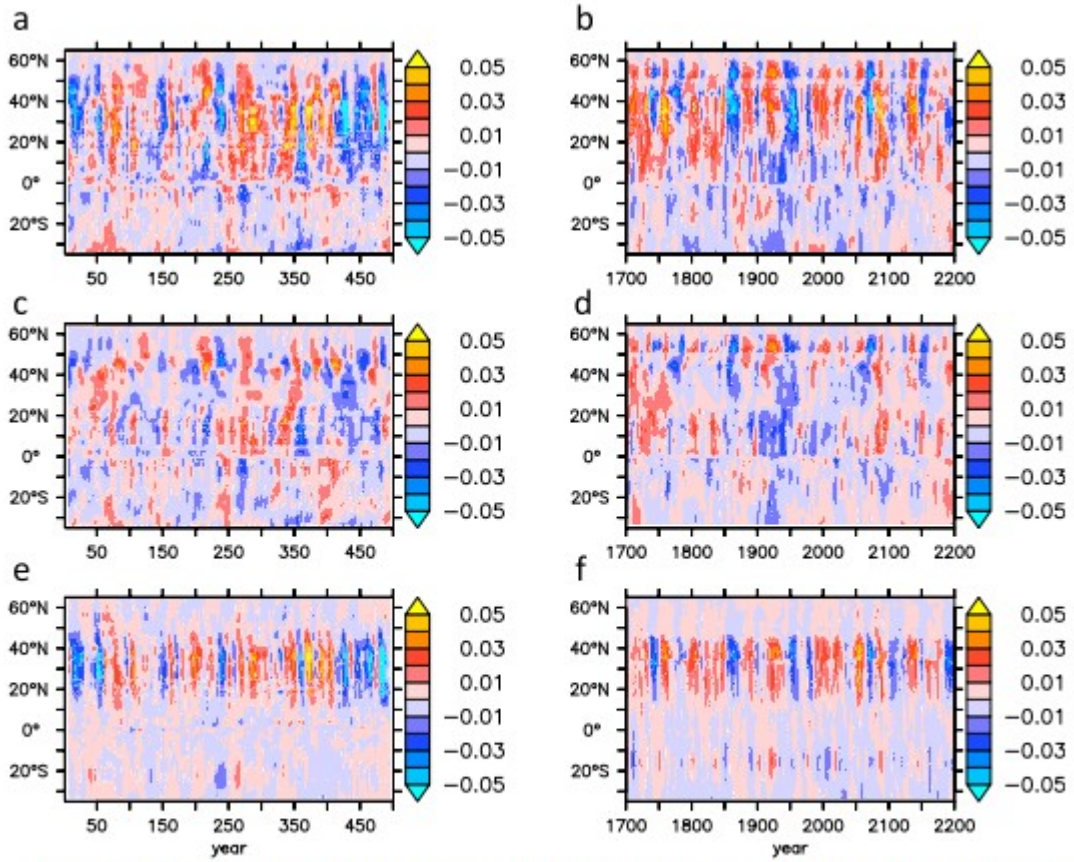

FIG. 6. Modeled Fov(y) anomalies (Sv) as a function of time and latitude in (a) ESM2M and (b) CESM1, and their contributions from (c),(d) salinity and (e),(f) velocity anomalies, respectively. Shown are 7-point running averages of the original annual time series with no meridional smoothing applied.

FIG. 6. Modeled Fov(y) anomalies (Sv) as a function of time and latitude in (a) ESM2M and (b) CESM1, and their contributions from (c),(d) salinity and (e),(f) velocity anomalies, respectively. Shown are 7-point running averages of the original annual time series with no meridional smoothing applied.

b. Basin-scale salt-advection feedback assumptions

As described in section 1, the basin-scale salt-advection feedback mechanism depends on three assumptions: 1) AMOC strength is influenced by the meridional density difference between the North Atlantic (NA) and South Atlantic (SA); 2) AMOC strength influences Fov at the Atlantic southern boundary; and 3) Fov at the Atlantic southern boundary then perturbs the meridional density difference, and therefore feeds back onto AMOC. We now examine the validity of these assumptions in the ESM2M and CESM1 control simulations. The NA (SA) domain is defined as the volume of seawater between 45° and 65°N (54° and 34°S), across the basin width for the NA, and between 53.3°W and 17.5°E for the SA, and from the surface to 4-km depth. In both models, the AMOC index at 45°N (AMOC45N herein) is significantly correlated with low-pass-filtered NA–SA density differences (Figs. 7a,b), and its thermal (Figs. 7c,d) as well as haline (Figs. 7e,f) contributions. Moreover, the NA water is warmer and saltier than the SA water; in other words, the thermal and haline effects contribute oppositely to the meridional density difference, with the haline effect being larger than that of the thermal effect (indicated by scales of the right ordinates in Figs. 7a–f).

Cross-spectral analysis between north–south density, temperature and salinity variations, and AMOC45N shows interesting phase relationships in the frequency domain (Figs. 7g,h). We will show shortly that variations in property gradient between the NA and SA domains are primarily controlled by NA variability while contributions from the SA are negligible; we therefore interpret these results in terms of variability in the subpolar North Atlantic. First, in both models, temperature and salinity variations are highly coherent on all time scales, with negligible phase lag (not shown). This is consistent with an advective mechanism where warm and salty subtropical waters are advected toward the subpolar North Atlantic by a variable AMOC. However, this inference is not conclusive, as any mechanism that accounts for synchronized changes in T and S in the subpolar North Atlantic could account for this behavior (including northward advection by the gyre circulation). Second, on shorter time scales, temperature variability dominates density variability, while on longer time scales salinity effects dominate (see Figs. 7g,h, where black dots are aligned with pink dots when $T < \sim$40 yr but approach blue dots on longer time scales). This is consistent with stronger damping of thermal than haline anomalies, which exposes salinity anomalies on longer time scales. Third, Figs. 7g and 7h show that, on decadal time scales, AMOC45N lags density variations in the subpolar North Atlantic, with a roughly 45°-phase difference. We interpret this phase lag of a few years as the time it takes for AMOC anomalies generated in the subpolar North Atlantic to propagate to 45°N (e.g., Zhang 2010). On these time scales, the phases of density variations (Figs. 7g,h, black dots) and their thermal contributions (Figs. 7g,h, pink dots) track each other closely, confirming thermal control of density. On multidecadal [$T =\sim$ (40–80) yr] and

centennial (T < ~80 yr) time scales, density variations are dominated by haline contributions (Figs. 7g,h, blue dots), with the phase difference between AMOC45N and density (Figs. 7g,h, black dots) being close to zero in ESM2M. In CESM1, however, this phase is small but systematically positive. This indicates that in CESM1, AMOC variability on multidecadal and centennial time scales leads density variations on these time scales in the subpolar North Atlantic.

As mentioned already, a closer look at the NA – SA density differences indicates that decadal and longer time-scale variability in these differences is controlled almost entirely by variability in the NA. Figure 8 compares the 11-yr low-pass-filtered NA – SA salinity difference to the separate NA and SA salinity in the ESM2M, CESM1, and EN4 observational data, all showing that the NA variability dominates the NA – SA difference on decadal and longer time scales. NA dominance is also found in the volume-averaged potential temperature difference between NA and SA across the ESMs and EN4 data (not shown), and in the relationship between AMOC and interhemispheric sea surface temperature dipole on multidecadal and centennial time scales across the CMIP5 models (Muir and Fedorov 2015). The NA dominance, combining with the high correlation between AMOC and NA – SA density difference, means that our results are consistent with previous studies where AMOC multidecadal variability is related to subpolar NA density–temperature– salinity variations (e.g., Danabasoglu 2008; Yeager and Danabasoglu 2014). It is worth noting that further examinations indicated that this NA dominance is not sensitive to how the NA and SA domains are defined exactly; halving the meridional extent of the domains, or using the surface to only 1-km depth still results in NA dominance (not shown).

We now search for possible relationships between AMOC variability in the North Atlantic and Fov, and in particular their time-scale dependence and meridional coherence, by performing spectral analysis on several key metrics. Figure 9 shows the expansion of the spectral energy of AMOC(y) and its meridional coherence in the frequency domain. ESM2M displays enhanced spectral power in the decadal band (Fig. 9a), while CESM1 only has a narrow peak around 40 yr (Fig. 9b). Both models display significantly enhanced spectral power at centennial time scales. The spectral properties of AMOC variability in these models are within the realm of other CMIP5 models (Muir and Fedorov 2017). The crossspectra between AMOC45N and AMOC(y) show to what extent AMOC variations are meridionally coherent (Figs. 9c,d). For CESM1, AMOC variability is meridionally coherent for multidecadal through centennial time scales (in agreement with Weijer and van Sebille 2014); for ESM2M AMOC is meridionally coherent for decadal and centennial time scales, but not for multidecadal time scales. Why ESM2M has reduced spectral power and no meridional coherence on these multidecadal time scales is not clear. The phase distributions of these cross-spectra (Figs. 9e,f) are consistent with southward propagation of AMOC signals, and suggest that an AMOC signal can reach 34°S within a decade for all time scales and in both models. This is consistent with a wave mechanism for the southward propagation of AMOC anomalies (e.g., Zhang 2010).

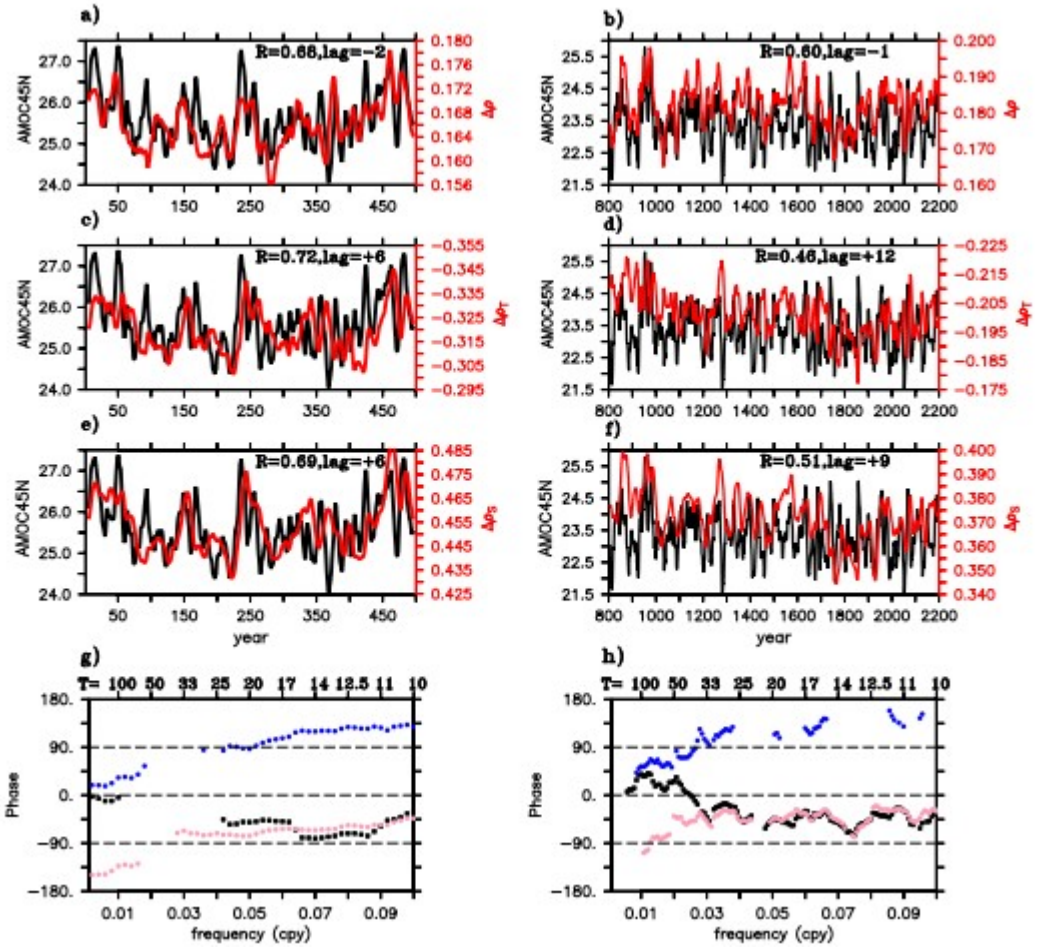

FIG. 7. Results from (left) ESM2M and (right) CESM1. (a)–(f) Eleven-point running averages of the annualmean AMOC index at 45°N (black lines; Sv) compared with NA minus SA density (kg m^{-3}) [red lines in (a)(b)] and its thermal [red lines in (c), (d)] as well as haline contributions [red lines in (e),(f)]; the maximum correlation coefficient and associated lag (positive means AMOC45N leads the other time series, and vice versa) between the shown time series are marked on the panel. Black (red) lines use the scale indicated by the left (right) ordinate. (g),(h) Phase from cross-spectrum between the unfiltered annual time series corresponding to the processes in (a), and (b) (black dots), (c) and (d) (pink dots), and (e) and (f) (blue dots); positive phase means AMOC45N leads the other time series. Spectral estimates are filtered with a 7-point Daniell filter; results that are statistically significant at 95% are shown.

How does the NA AMOC perturb Fov in the ESM simulations? Figures 10a and 10b show that the meridional coherence of AMOC does not automatically translate into a measurable impact of AMOC variability on Fov(y). In both models, AMOC strongly influences Fov in the North Atlantic, with an approximate antiphase relationship (Figs. 10c,d). However, in ESM2M this coherence does not extend south of about 15°N, showing that transport shear associated with basinwide AMOC variability does not influence meridional freshwater transport (in agreement with the small

contribution of the y0 term to Fov in Fig. 5a). In CESM1, support for an AMOC contribution to Fov is a bit stronger: significant coherences are found just south of the equator, and south of 20°S, on multidecadal to centennial time scales. It is possible that higher noise levels in Fov (e.g., due to wind driven processes) obscure the coherence in intervening latitude bands. In CESM1, the phase relationship between AMOC45N and Fov(y) is roughly the same as between AMOC45N and AMOC(y), supporting the notion that basinwide AMOC variability affects meridional freshwater transport in the South Atlantic to a certain degree (as also suggested by the more significant contribution of the y0 term to Fov in Fig. 5b).

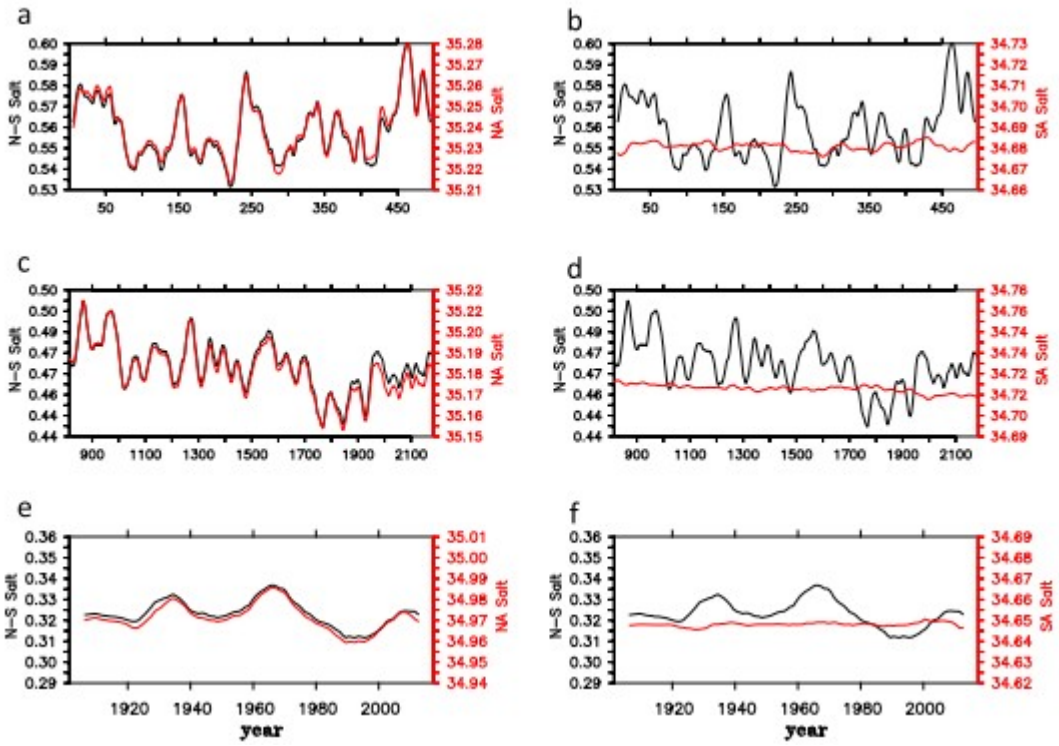

FIG. 8. (a),(b) ESM2M-simulated NA–SA salinity difference [black lines; left ordinate scales in (a) and (b); psu] and the NA-averaged salinity [red line; right ordinate scale in (a); psu] as well as SA-averaged salinity [red line; right ordinate scale in (b); psu]. (c),(d) As in (a),(b), but from the CESM1. (e),(f) As in (a),(b), but from the EN4 data. Shown are 11-point running averages of annual time series of each variable.

Another possible impact of AMOC variability on Fov is through modification of the salinity profile in the South Atlantic. Figures 10e–h show the coherence and phase between AMOC45N and salinity, zonally averaged across the Atlantic and vertically between 1- and 3-km depth (roughly corresponding to the southward moving North Atlantic Deep Water layer of AMOC). In ESM2M, this coherence is very sporadic on decadal time scales (T < ~30 yr), with no consistency in its meridional structure, suggesting that AMOC variability is not systematically related to salinity anomalies in its lower branch. In contrast, CESM1 shows coherence on multidecadal to centennial time scales throughout most of the Atlantic, with the phase distribution suggesting slow southward propagation (30-yr transit time from 45°N to 34°S; an

advective time scale), and a strong AMOC at 45°N is associated with relatively fresh conditions at depth, suggested by the 180° phase values around 45°N. To summarize, in ESM2M, Fov is not influenced much by basin-scale variability in AMOC, nor by any AMOCrelated salinity variations. In contrast, in CESM1, basinwide AMOC variability affects Fov to a certain degree, and there is also some evidence for basinwide changes in the lower-layer salinity associated with AMOC fluctuations. However, the latter's effect on vertically integrated Fov seems to be diminished by salinity variability in the upper ocean (judging by the weaker coherence in Fig. 10b than in Fig. 10f).

Finally, we explore if we can find evidence for natural variability of Fov affecting the salinity stratification in the Atlantic Ocean, and hence AMOC. Figures 11a–d show that there is hardly any relationship between Fov and AMOC(y) in ESM2M, consistent with Fig. 10a. The sole exception is a very narrow band around the 20-yr time scale, which corresponds to the time scale of enhanced AMOC energy (Fig. 9a). The negative phase at this time scale indicates that Fov lags, rather than leads, AMOC variability. In CESM1, on the other hand, there is significant coherence on a wide range of time scales; but again, the phase relationship is mostly negative, indicating that Fov in general lags AMOC variability. Note that the coherence between Fov and AMOC(y) (Figs. 11a,b) displays more meridional consistency than the coherence between AMOC45N and Fov(y) (Figs. 10a,b), if only for the 20-yr time scale in ESM2M and centennial time scales in CESM1. This may indicate that Fov(y) is noisier than AMOC(y), and that this noise may hide some relevant signal in Figs. 10a and 10b.

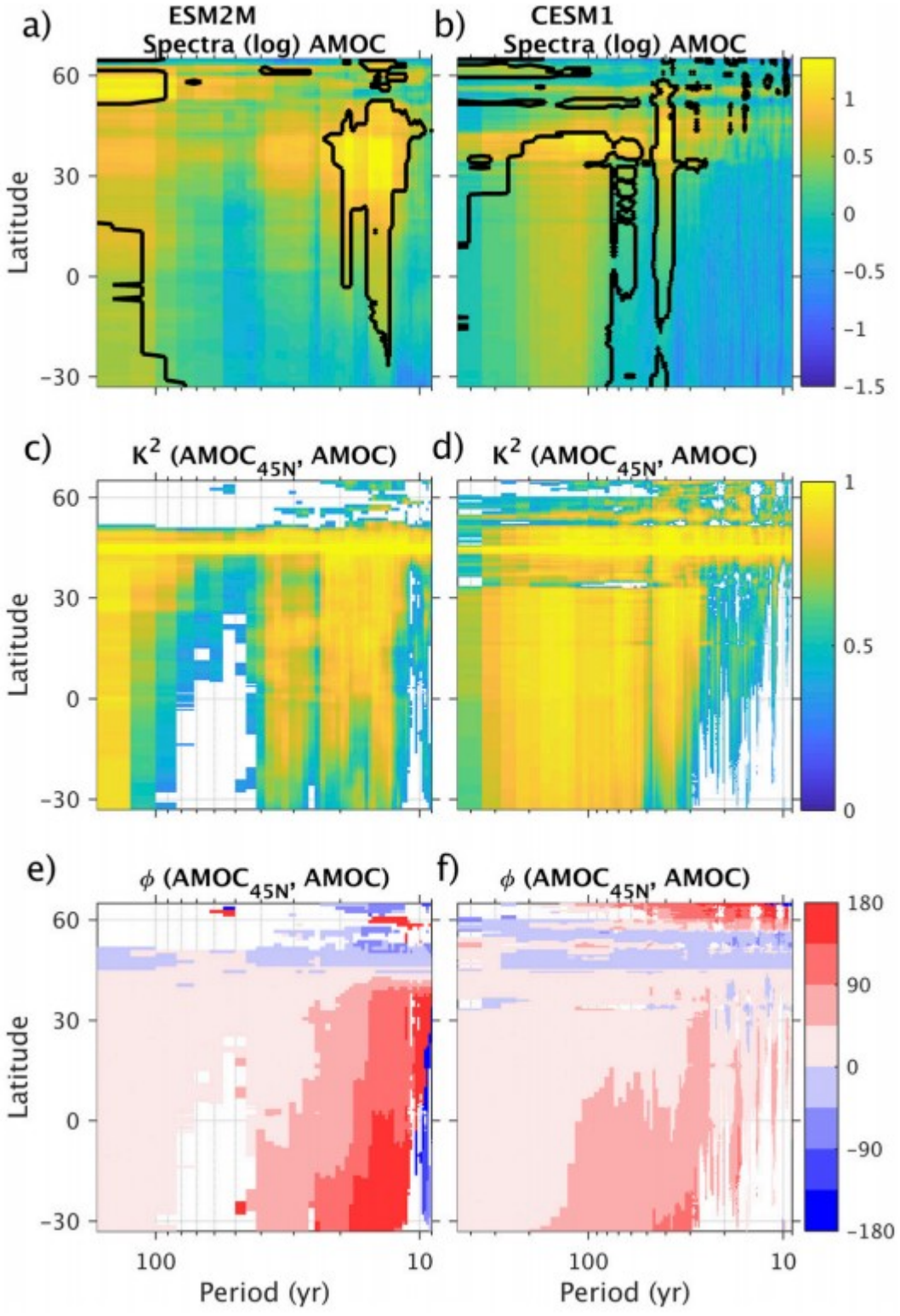

FIG. 9. Spectral analysis of AMOC in (left) ESM2M and (right) CESM1 vs latitude. (a), (b) Logarithm of spectral energy of AMOC(y). Black contours indicate where the spectra differ from a red-noise process with 90% confidence. (c),(d) Squared

coherence and (e),(f) coherence phase between AMOC45N and AMOC(y). Positive (negative) phase means AMOC45N leads (lags) AMOC(y). Values are only plotted where coherence is significant at 90%. Significance is tested against the 90th percentile of 1000 synthetic time series with the same first-order autoregressive (AR-1) characteristics as the best fit to the original time series. Spectral estimates are filtered with a 7-point Daniell filter (von Storch and Zwiers 1999).

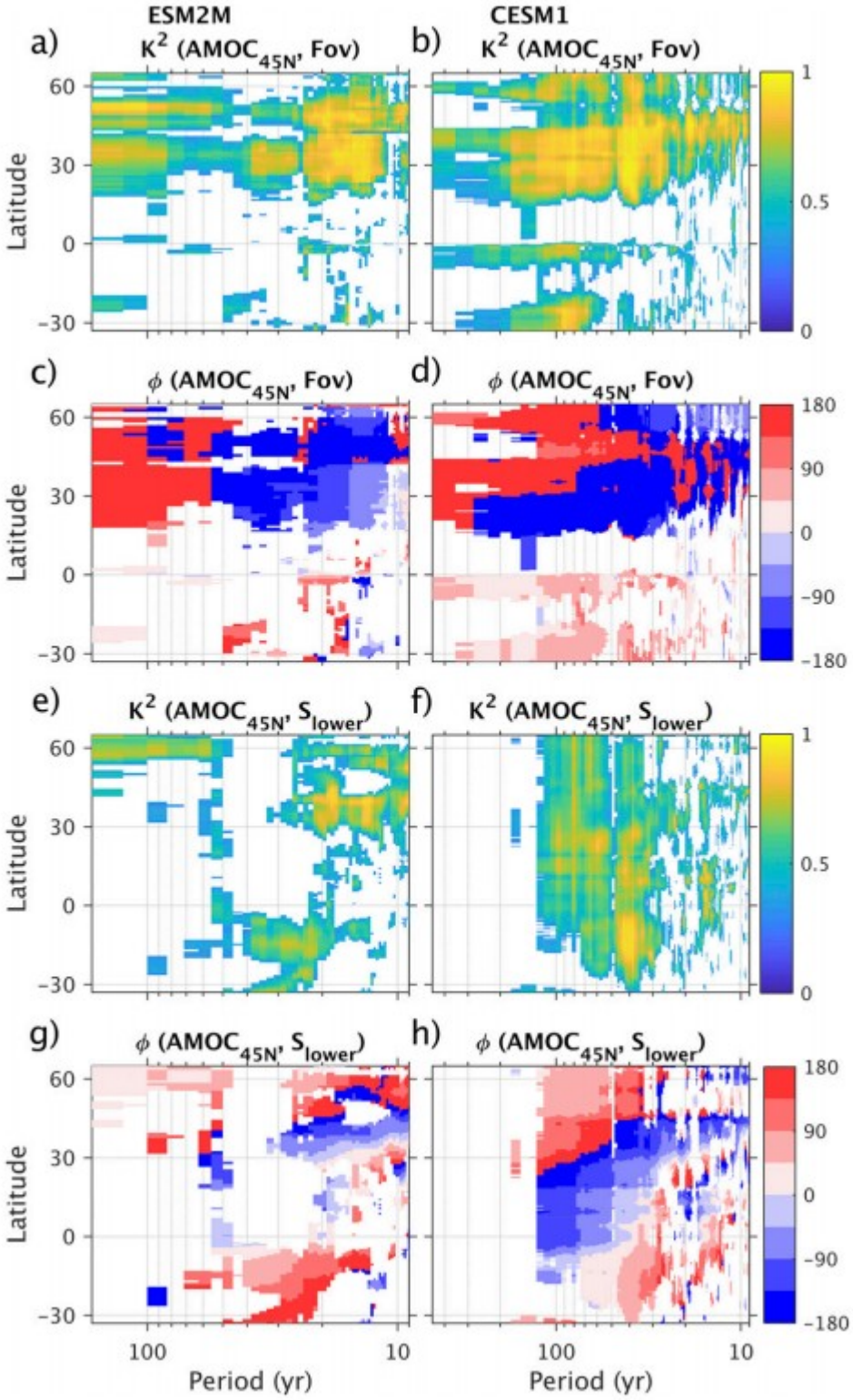

FIG. 10. Squared coherence and coherence phase between AMOC45N and (a)–(d) Fov(*y*) and (e)–(h) lower-layer salinity (salinity averaged zonally across the Atlantic, and between 1 and 3 km depth). Positive (negative) phase means AMOC45N leads

(lags) the field. Values are only plotted where coherence is significant at 90%. Significance is tested against the 90th percentile of 1000 synthetic time series with the same AR-1 characteristics as the best fit to the original time series. Spectral estimates are filtered with a 7-point Daniell filter (von Storch and Zwiers 1999).

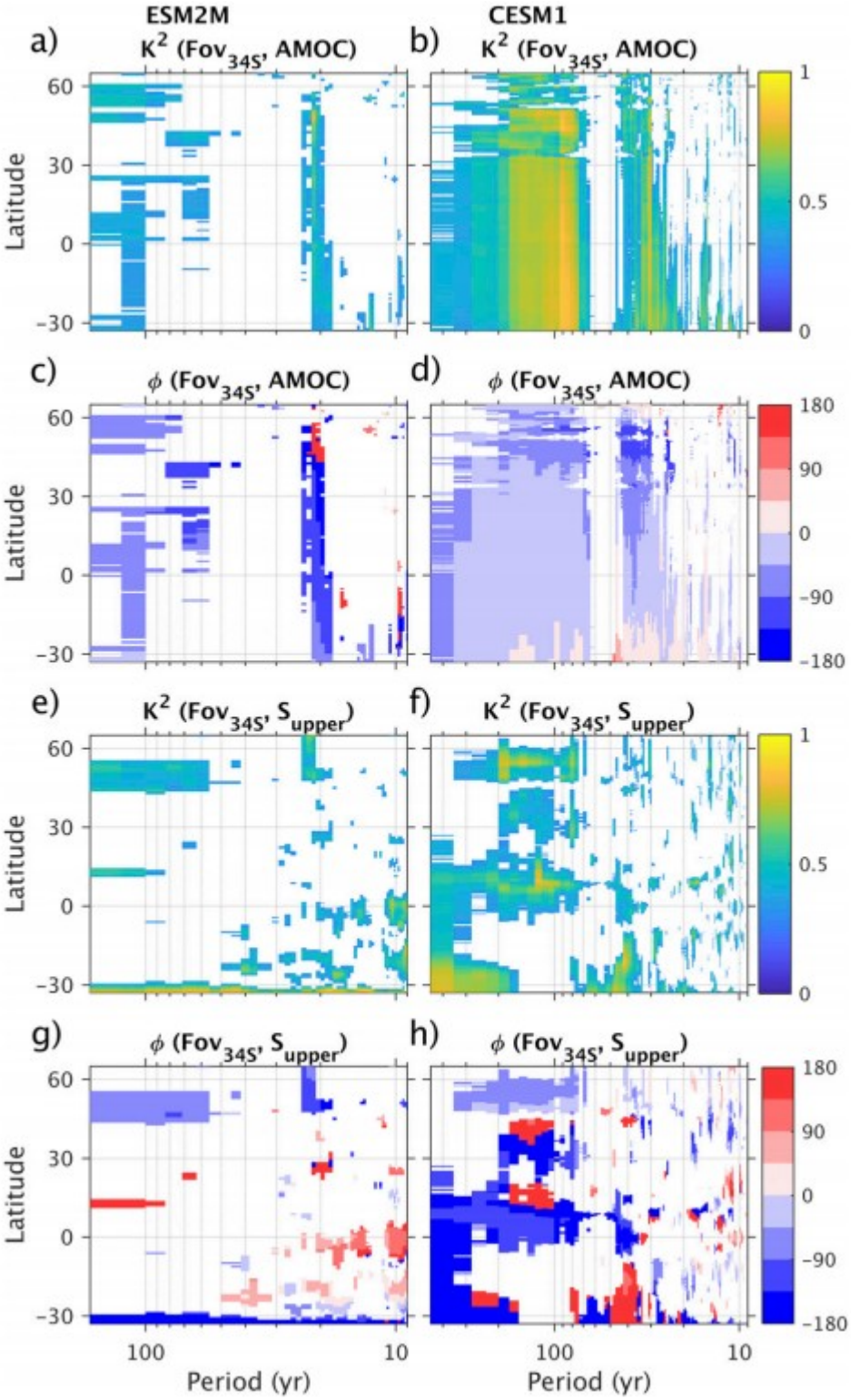

FIG. 11. As in Fig. 10, but for the coherence between Fov and (a)–(d) AMOC(y) and (e)–(h) upperlayer salinity (salinity averaged zonally across the Atlantic, and between 100 m and 1 km depth). Positive (negative) phase means Fov leads (lags) the field.

It is possible that fluctuations in Fov only impact AMOC in the North Atlantic when the salinity anomalies generated by Fov anomalies arrive in the subpolar North Atlantic. To test this hypothesis, we also calculate the coherence between Fov and zonally averaged upperlayer salinity in the Atlantic (Figs. 11e–h). In ESM2M, Fov is only coherent with the upper-layer salinity at 34°S, showing that Fov is determined by local, rather than basin-scale, salinity variability. In CESM1, significant coherence is a bit more widespread, with an antiphase relationship between Fov and upper-layer salinity, as expected. However, there is little meridional consistency in the spatial distribution, and no meaningful deviations from the antiphase relationship that would suggest northward propagation. Furthermore, for the time scales on which Fov is most strongly influenced by AMOC variability (80–200 yr; Fig. 11b), no salinity variations appear to be generated in the South Atlantic (Fig. 11h). Hence, based on an analysis of natural variability in two ESMs, there is no evidence to support the assumption that variability in Fov leads to significant changes in the Atlantic salinity distribution, or ultimately in AMOC.

4. Summary and discussion

The term ‘‘salt advection feedback’’ refers to a feedback between AMOC, the meridional advection of salt, and the meridional density gradient. On the scale of the North Atlantic, northward transport of salty, subtropical waters is thought to precondition the subpolar North Atlantic for deep convection, thus stimulating AMOC and representing a positive feedback. However, the feedback has received a lot of attention in the context of the entire Atlantic Ocean, as the sign of the AMOCinduced freshwater transport across 34°S (i.e., Fov) has been suggested as an indicator of AMOC stability. The basin-scale salt-advection feedback has its origin in simple box models (Fig. 12a shows a schematic), but how applicable it is to the more complex climate system deserves scrutiny. For example, while it is known that the solution branches of box models are located in distinct dynamical regimes separated by the sign of Fov, it is often overlooked that these dynamical regimes are also distinguishable by their ‘‘forcing’’ characteristics. Specifically, Eq. (1) in Rahmstorf (1996) demands that when Fov is positive [note that Fov has the opposite sign of parameter ‘‘F1’’ in Rahmstorf (1996) representing the atmospheric freshwater transport], the NA box is saltier than the SA box, and the corresponding solution branches must be ‘‘haline-’’ (or thermohaline-) driven; conversely, when Fov is negative, the NA box is fresher than the SA box, and the solution branch must be ‘‘thermally’’ driven, and only the ‘‘thermally’’ driven solutions have multiple equilibria. In observations and the ESM simulations, the NA is saltier and warmer than the SA (Figs. 7 and 8), and by this measure, the modern AMOC ‘‘on’’ state is ‘‘haline’’-driven. However, the observed Fov is likely negative (Weijer et al. 1999; McDonagh and King 2005; Bryden et al. 2011; Garzoli et al. 2013), and the salinity bias– corrected Fov at this latitude in the ESMs is also negative (Figs. 2c,d; Mecking et al. 2017). In other words, the realworld situation of a ‘‘haline’’-driven AMOC with

negative Fov is not permissible by the box model construction. It should come as no surprise that the real climate system, containing feedbacks not captured by the box model, could be governed by different dynamics than the box models [see, e.g., Wolfe and Cessi (2015) for a different paradigm].

At face value, the conceptual relationships between AMOC amplitude and NA–SA density difference are found in the ESM simulations (Figs. 7a,b). A closer examination reveals that the decadal and longer time-scale variability in the north–south density difference is controlled almost entirely by NA density fluctuations, in both ESMs and ocean observations (Fig. 8). The weak correlations between SA property changes and AMOC variability implies strong water mass property changes along the NADW pathway, including its final upwelling in the Southern Ocean. On the other hand, the robust and highly significant correlations between NA property and AMOC variability suggest that processes pertaining to the North Atlantic region are the most important forcing mechanism for AMOC variability on these scales.

The univariate spectra of AMOC(y) and cross-spectra between AMOC45N and AMOC(y) in ESM2M and CESM1 confirm strong meridional coherence in AMOC(y), albeit with different characteristic time scales across the models. In CESM1, AMOC is meridionally coherent for multidecadal and centennial time scales, while in ESM2M meridional coherence is found in decadal and centennial bands (Fig. 9). However, the coherence between AMOC45N and Fov(y) south of 15°N is not very robust, and a significant signal extends to 34°S only in CESM1 (Fig. 10). This result differs from Mecking et al. (2017, their Fig. 5) where the intermodel correlation between time-mean AMOC(26.5°N) and Fov(y) in the South Atlantic is high. We hypothesize that AMOCrelated signals south of 15°N are easily obscured by other variability that is not associated with AMOC, like variations in the upper-ocean salinity or the shallow wind-driven cells in the subtropics. Also, we did not find evidence to support the notion that Fov(y) from the South Atlantic feeds back on AMOC in the North Atlantic. Wherever there is significant coherence between Fov(y) south of 15°N and AMOC45N, or between Fov and AMOC(y), AMOC45N consistently leads Fov (Figs. 10c,d and 11c,d). In addition, the influence of Fov on upper-layer salinity anomalies does not extend into the North Atlantic (Figs. 11e–h). Taken together, these results suggest that the internal variability of Fov in these models is not able to generate significant perturbations in the stratification of the Atlantic Ocean.

Based on the above ESM results, we provide a revised version of the salt-advection feedback schematic in Fig. 12b. The link from AMOC to Fov in the South Atlantic could occur via two mechanisms: change in meridional velocity vertical structure (which works on the modeled mean salinity with biases) and change in salinity distributions. AMOC has strong meridional coherence from NA to SA, but Fov is only weakly influenced by local meridional velocity. On the other hand, in CESM1, NA AMOC impacts basin-scale lower-layer salinity distribution to some extent, although the latter’s role on vertically integrated Fov is limited by processes happening in the upper ocean. We do not find any evidence to support a link between Fov and the NA – SA density difference in both models. Last, the relationship between AMOC(45°N) and north–south density gradient (which is dominated by subpolar NA density

variations) is time scale– and process-dependent: on shorter time scales (T < 40–50 yr), the thermal control on density and hence AMOC variability dominates, which then transitions to haline control dominating on longer time scales.

It is worth mentioning that both models considered here (as most IPCC class models; Drijfhout et al. 2011; Weaver et al. 2012) have Fov > 0, but it is likely that our conclusions also hold for models that have a positive salt-advection feedback through Fov < 0, as the processes responsible for the meridional propagation of signals would be exactly the same. It must be noted, though, that even in models that have a positive saltadvection feedback, a large-amplitude perturbation would be required to trigger a collapse. Even in simple box models, other feedbacks (mostly negative) are active that dominate the salt-advection feedback for small perturbations; in particular the ys0 and y0 s0 terms in Eq. (2), and the temperature advection feedback. We acknowledge that the fact that our analysis was not able to identify the basin-scale salt-advection feedback in natural variability does not rule out that this feedback may be excited by a strong enough freshwater perturbation. Our analysis does not allow us to make a general statement about AMOC bistability in these models, but it allows for examinations of salt-advection feedback mechanisms associated with internal variability of AMOC.

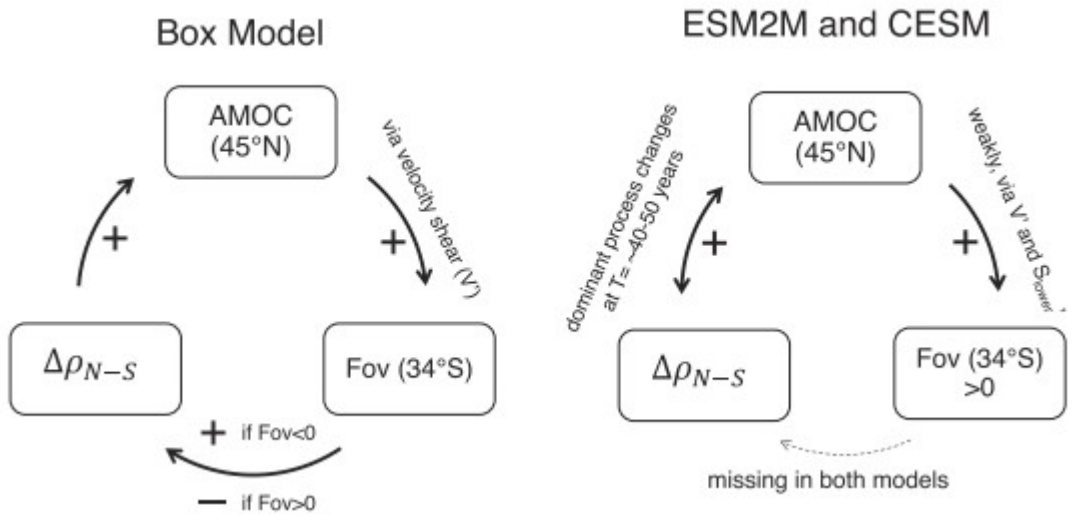

FIG. 12. Physical links underlying the basin-scale salt-advection feedback as envisioned by box models and their counterparts in ESM simulations. In both panels, rectangles represent (clockwise from the top) AMOC at 45°N (used as an AMOC index), Fov(y) at 34°S, and NA–SA density difference ($\Delta\rho_{N\text{–}S}$), respectively. Arrows represent forcing from one variable to the next, with the + or – signs indicating if the forcing effect is positive or negative. Based on (left) box models, stronger AMOC at 45°N increases Fov by changing the velocity shear at 34°S, and therefore the arrow connecting them is marked as positive. The forcing from Fov to $\Delta\rho_{N\text{–}S}$ can be either positive or negative depending on the sign of Fov: when Fov < 0, stronger Fov increases $\Delta\rho_{N\text{–}S}$ (because more freshwater is transferred out of the Atlantic Ocean), and therefore the arrow is positive; when Fov > 0, stronger Fov decreases $\Delta\rho_{N\text{–}S}$ (because more freshwater is transferred into the Atlantic Ocean), and the arrow is therefore negative; last, stronger $\Delta\rho_{N\text{–}S}$ strengthens AMOC, another positive

link. Together, these links form a closed feedback loop; in particular, a negative Fov allows for continuous positive effect to propagate around the loop, destabilizing AMOC, whereas a positive Fov breaks the continuous positive forcing around the loop, stabilizing AMOC. (right) This conceptual model is revised based on analyses on internal variability of AMOC in full ESM simulations where it is found that 1) AMOC45N influences Fov only weakly through either the velocity shear or lower-layer salinity distributions; 2) effect from Fov on $\Delta\rho_{N\text{–}S}$ is not detected in both ESMs; and 3) the relationship between AMOC45N and $\Delta\rho_{N\text{–}S}$ (the latter is almost entirely controlled by subpolar NA density variations with negligible contributions from SA) is time scale– and process-dependent: on decadal and multidecadal time scales (T < 40–50 yr), AMOC variability lags the thermal effect–dominated density variation in both models; on longer time scales (T > 40–50 yr), density variation is dominated by the haline effect, and AMOC variability lags density variation in ESM2M but leads it in CESM1 (hence, we draw a double pointed arrow between AMOC45N and $\Delta\rho_{N\text{–}S}$).

To ultimately prove the existence of multiple equilibria of AMOC under present-day forcing conditions in a model, it is necessary to show that AMOC can be made to transition abruptly to a stable ‘‘off’’ state by a large-amplitude but finite-time perturbation of the system. Alternatively, one could try to determine hysteresis behavior, by gradually increasing the surface flux perturbation until a collapsed state is reached, and then showing that this ‘‘off’’ state is maintained when reducing this perturbation back to zero. To the best of our knowledge, thus far AMOC hysteresis has only been demonstrated in earth system models of intermediate complexity (EMICs) and one climate model with very coarse horizontal resolution (Rahmstorf et al. 2005; Hawkins et al. 2011) because this type of experiment is computationally too costly to be carried out routinely. If a metric as simple as Fov could indicate whether a stable ‘‘off’’ state coexists with a strong AMOC ‘‘on’’ state, it would be valuable. Nonetheless, Fov does not indicate how strong a perturbation needs to be to trigger a transition between equilibria. In that sense, the more relevant threshold is the point beyond which a strong overturning ‘‘on’’ state can no longer be maintained. Thus far, no reliable metric has been found to identify this point.

5. Conclusions

In this paper, we investigated whether evidence for the basin-scale salt-advection feedback mechanisms could be found in realistic ESMs by studying internal variability in two global ESM preindustrial control simulations. There are six main conclusions from this study. The first and third have been documented previously, but we believe the other ones are new.

The sign of Fov(y) in the South Atlantic is determined primarily by the local salinity distribution in both the initial adjustment phase and quasi-equilibrium state of the ESM simulations. Both the upper ocean above 800 m and deep ocean between 1.2 and 4 km contribute to a positive Fov(y) bias in the South Atlantic. This supports results in Cimatoribus et al. (2012), Jackson (2013), and Mecking et al. (2017).

Decadal and longer time-scale variability of Fov(y) in the ESM simulations is dominated by variability in salinity rather than in the velocity field everywhere in the Atlantic outside of the northern subtropics (20°–45°N).

Decadal and longer time-scale AMOC variability is highly correlated with north–south density variability, and this variability is almost entirely controlled by variability in the North Atlantic density. This supports results in Griesel and Maqueda (2006), Danabasoglu (2008), and de Boer et al. (2010).

Density variation in the subpolar North Atlantic is controlled by thermal, rather than saline, anomalies on decadal and shorter time scales. Only on multidecadal and longer time scales (T > 40–50 yr) does salinity dominate density variability.

The direct effect of AMOC on Fov in the South Atlantic through perturbing the region's velocity shear is detectable but weak for internal variability; also, there are suggestions that AMOC influences Fov indirectly through its impact on salinity in the southward limb, and subsequent changes in the salinity stratification at 34°S, but again, this signal is weak.

In the context of internal decadal to centennial timescale variability, feedbacks from Fov in the South Atlantic on AMOC in the North Atlantic cannot be detected. This is the missing link in the revised schematic in Fig. 12b, and prevents the feedback loop from closing for internal variability.

Our next step is to quantify the freshwater budget terms and their spatiotemporal variability throughout the Atlantic, and to examine how they are influenced by, and in turn may feed back on, AMOC. Consistent with previous studies, our results emphasize that density variation in the NA is key to AMOC decadal and centennial time-scale variability. What processes control this density variation and how the answer to this question may depend on modeling parameters are not fully understood. In addition, targeted numerical experiments where AMOC is forced to change more systematically than the natural variability amplitude in control runs may shed more light on the mechanisms involved, which would then help to model these processes better, and eventually to predict more accurately future AMOC changes.

Acknowledgments. This research is supported by the National Oceanic and Atmospheric Administration (NOAA) Climate Program Office under Climate Variability and Predictability Program Grants NA16OAR4310169, NA16OAR4310170, and NA16OAR4310171; Regional and Global Climate Modeling Program (RGCM) of the U.S. Department of Energy (DOE)'s Office of Science (BER) through support of the HiLAT project; and partially by the National Science Foundation (NSF) Collaborative Research EaSM2 Grant OCE-1243015. NCAR is sponsored by the NSF. The NSF and DOE BER RGCM support the CESM project. Computing resources were provided by the Climate Simulation Laboratory at NCAR's Computational and Information Systems Laboratory, sponsored by the NSF. We thank Drs. Andrea Cimatoribus, Sybren Drijfhout, and Yavor Kostov for their insightful comments, which improved the final version of the manuscript. This is JISAO contribution 2017-0121 and PMEL contribution 4729.

REFERENCES

Bryden, H. L., B. A. King, and G. D. McCarthy, 2011: South Atlantic overturning circulation at 248S. J. Mar. Res., 69, 38–55, https://doi.org/10.1357/002224011798147633.

Butler, E. D., K. I. C. Oliver, J. J.-M. Hirschi, and J. V. Mecking, 2016: Reconstructing global overturning from meridional density gradients. Climate Dyn., 46, 2593–2610, https://doi.org/ 10.1007/s00382-015-2719-6.

Cimatoribus, A. A., S. S. Drijfhout, M. den Toom, and H. A. Dijkstra, 2012: Sensitivity of the Atlantic meridional overturning circulation to South Atlantic freshwater anomalies. Climate Dyn., 39, 2291–2306, https://doi.org/10.1007/s00382-012-1292-5.

——, ——, and H. A. Dijkstra, 2014: Meridional overturning circulation: Stability and ocean feedbacks in a box model. Climate Dyn., 42, 311–328, https://doi.org/10.1007/s00382-012-1576-9.

Danabasoglu, G., 2008: On multidecadal variability of the Atlantic meridional overturning circulation in the Community Climate System Model version 3. J. Climate, 21, 5524–5544, https:// doi.org/10.1175/2008JCLI2019.1.

de Boer, A. M., A. Gnanadesikan, N. R. Edwards, and A. J. Watson, 2010: Meridional density gradients do not control the Atlantic overturning circulation. J. Phys. Oceanogr., 40, 368– 380, https://doi.org/10.1175/2009JPO4200.1.

den Toom, M., H. A. Dijkstra, W. Weijer, M. W. Hecht, M. E. Maltrud, and E. van Sebille, 2014: Response of a strongly eddying global ocean model to North Atlantic freshwater perturbations. J. Phys. Oceanogr., 44, 464–481, https://doi.org/ 10.1175/JPO-D-12-0155.1.

de Vries, P., and S. L. Weber, 2005: The Atlantic freshwater budget as a diagnostic for the existence of a stable shut down of the meridional overturning circulation. Geophys. Res. Lett., 32, L09606, https://doi.org/10.1029/2004GL021450.

Dijkstra, H. A., 2007: Characterization of the multiple equilibria regime in a global ocean model. Tellus, 59A, 695–705, https:// doi.org/10.1111/j.1600-0870.2007.00267.x.

Drijfhout, S. S., S. L. Weber, and E. van der Swaluw, 2011: The stability of the MOC as diagnosed from model projections for pre-industrial, present and future climates. Climate Dyn., 37, 1575–1586, https://doi.org/10.1007/s00382-010-0930-z.

Dunne, J. P., and Coauthors, 2012: GFDL’s ESM2 global coupled climate–carbon Earth system models. Part I: Physical formulation and baseline simulation characteristics. J. Climate, 25, 6646–6665, https://doi.org/10.1175/JCLI-D-11-00560.1.

Garzoli, S. L., M. O. Baringer, S. Dong, R. C. Perez, and Q. Yao, 2013: South Atlantic meridional fluxes. Deep-Sea Res. I, 71, 21–32, https://doi.org/10.1016/j.dsr.2012.09.003.

Gent, P. R., 2018: A commentary on the Atlantic meridional overturning circulation stability in climate models. Ocean Modell., 122, 57–66, https://doi.org/10.1016/j.ocemod.2017.12.006.

Gnanadesikan, A., 1999: A simple predictive model for the structure of the oceanic pycnocline. Science, 283, 2077–2079, https://doi.org/10.1126/science.283.5410.2077.

Gordon, A. L., 1986: Interocean exchange of thermocline water. J. Geophys. Res., 91, 5037–5046, https://doi.org/10.1029/ JC091iC04p05037.

Griesel, A., and M. A. M. Maqueda, 2006: The relation of meridional pressure gradients to North Atlantic deep water volume transport in an ocean general circulation model. Climate Dyn., 26, 781–799, https://doi.org/10.1007/s00382-006-0122-z.

Hawkins, E., R. S. Smith, L. C. Allison, J. M. Gregory, T. J. Woolings, H. Pohlmann, and B. de Cuevas, 2011: Bistability of the Atlantic overturning circulation in a global climate model and links to ocean freshwater transport. Geophys. Res. Lett., 38, L10605, https://doi.org/10.1029/2011GL047208; Corrigendum, 38, L16699, https://doi.org/10.1029/2011GL048997.

Huisman, S. E., M. den Toom, H. A. Dijkstra, and S. S. Drijfhout, 2010: An indicator of the multiple equilibria regime of the Atlantic meridional overturning circulation. J. Phys. Oceanogr., 40, 551–567, https://doi.org/10.1175/2009JPO4215.1.

Jackson, L. C., 2013: Shutdown and recovery of the AMOC in a coupled global climate model: The role of the advective feedback. Geophys. Res. Lett., 40, 1182–1188, https://doi.org/ 10.1002/grl.50289.

Johnson, H. L., D. P. Marshall, and D. A. J. Sproson, 2007: Reconciling theories of a mechanically driven meridional overturning circulation with thermohaline forcing and multiple equilibria. Climate Dyn., 29, 821–836, https://doi.org/10.1007/s00382-007-0262-9.

Kay, J. E., and Coauthors, 2015: The Community Earth System Model (CESM) large ensemble project: A community resource for studying climate change in the presence of internal climate variability. Bull. Amer. Meteor. Soc., 96, 1333–1349, https://doi.org/10.1175/BAMS-D-13-00255.1.

Levitus, S., and Coauthors, 1998: Introduction. Vol. 1, World Ocean Database 1998, NOAA Atlas NESDIS 18, 346 pp.

Liu, W., and Z. Liu, 2013: A diagnostic indicator of the stability of the Atlantic meridional overturning circulation in CCSM3. J. Climate, 26, 1926–1938, https://doi.org/10.1175/JCLI-D-11-00681.1.

——, and ——, 2014: A note on the stability indicator of the Atlantic meridional overturning circulation. J. Climate, 27, 969– 975, https://doi.org/10.1175/JCLI-D-13-00181.1.

——, ——, and E. C. Brady, 2014: Why is the AMOC monostable in coupled general circulation models? J. Climate, 27, 2427– 2443, https://doi.org/10.1175/JCLI-D-13-00264.1.

McDonagh, E. L., and B. A. King, 2005: Oceanic fluxes in the South Atlantic. J. Phys. Oceanogr., 35, 109–122, https://doi.org/ 10.1175/JPO-2666.1.

Mecking, J. V., S. S. Drijfhout, L. C. Jackson, and T. Graham, 2016: Stable AMOC off state in an eddy-permitting coupled climate model. Climate Dyn., 47, 2455–2470, https://doi.org/10.1007/ s00382-016-2975-0.

——, ——, ——, and M. B. Andrews, 2017: The effect of model bias on Atlantic freshwater transport and implications for AMOC bi-stability. Tellus, 69A, 1299910, https://doi.org/ 10.1080/16000870.2017.1299910.

Muir, L. C., and A. V. Fedorov, 2015: How the AMOC affects ocean temperatures on decadal to centennial timescales: The North Atlantic versus an interhemispheric seesaw. Climate Dyn., 45, 151–160, https://doi.org/10.1007/s00382-014-2443-7.

——, and ——, 2017: Evidence of the AMOC interdecadal mode related to westward propagation of temperature anomalies in CMIP5 models. Climate Dyn., 48, 1517–1535, https://doi.org/ 10.1007/s00382-016-3157-9.

Rahmstorf, S., 1996: On the freshwater forcing and transport of the Atlantic thermohaline circulation. Climate Dyn., 12, 799–811, https://doi.org/10.1007/s003820050144.

——, and Coauthors, 2005: Thermohaline circulation hysteresis: A model intercomparison. Geophys. Res. Lett., 32, L23605, https://doi.org/10.1029/2005GL023655.

Rooth, C., 1982: Hydrology and ocean circulation. Prog. Oceanogr., 11, 131–149, https://doi.org/10.1016/0079-6611(82)90006-4.

Sijp, W. P., M. H. England, and J. M. Gregory, 2012: Precise calculations of the existence of multiple AMOC equilibria in coupled climate models. Part I: Equilibrium states. J. Climate, 25, 282–298, https://doi.org/10.1175/2011JCLI4245.1.

Steele, M., R. Morley, and W. Ermold, 2001: PHC: A global ocean hydrography with a high-quality Arctic Ocean. J. Climate, 14, 2079–2087, https://doi.org/10.1175/1520-0442(2001)014,2079: PAGOHW.2.0.CO;2.

Stommel, H., 1961: Thermohaline convection with two stable regimes of flow. Tellus, 13, 224–230, https://doi.org/10.3402/ tellusa.v13i2.9491.

Toggweiler, J. R., and B. Samuels, 1998: On the ocean’s large-scale circulation near the limit of no vertical mixing. J. Phys. Oceanogr., 28, 1832–1852, https://doi.org/10.1175/ 1520-0485(1998)028,1832:OTOSLS.2.0.CO;2.

von Storch, H., and F. W. Zwiers, 1999: Statistical Analysis in Climate Research. Cambridge University Press, 484 pp. Weaver, A. J., and Coauthors, 2012: Stability of

the Atlantic meridional overturning circulation: A model intercomparison. Geophys. Res. Lett., 39, L20709, https://doi.org/10.1029/ 2012GL053763.

Weijer, W., and E. van Sebille, 2014: Impact of Agulhas leakage on the Atlantic overturning circulation in the CCSM4. J. Climate, 27, 101–110, https://doi.org/10.1175/JCLI-D-12-00714.1.

——, W. P. M. de Ruijter, H. A. Dijkstra, and P. J. van Leeuwen, 1999: Impact of interbasin exchange on the Atlantic overturning circulation. J. Phys. Oceanogr., 29, 2266–2284, https://doi.org/ 10.1175/1520-0485(1999)029,2266:IOIEOT.2.0.CO;2.

——, ——, A. Sterl, and S. S. Drijfhout, 2002: Response of the Atlantic overturning circulation to South Atlantic sources of buoyancy. Global Planet. Change, 34, 293–311, https://doi.org/ 10.1016/S0921-8181(02)00121-2.

Wijffels, S. E., R. W. Schmitt, H. L. Bryden, and A. Stigebrandt, 1992: Transport of freshwater by the oceans. J. Phys. Oceanogr., 22, 155–162, https://doi.org/10.1175/1520-0485(1992)022,0155: TOFBTO.2.0.CO;2.

Wolfe, C. L., and P. Cessi, 2014: Salt feedback in the adiabatic overturning circulation. J. Phys. Oceanogr., 44, 1175–1194, https://doi.org/10.1175/JPO-D-13-0154.1.

——, and ——, 2015: Multiple regimes and low-frequency variability in the quasi-adiabatic overturning circulation. J. Phys. Oceanogr., 45, 1690–1708, https://doi.org/10.1175/ JPO-D-14-0095.1.

Yeager, S., and G. Danabasoglu, 2014: The origins of late-twentiethcentury variations in the large-scale North Atlantic circulation. J. Climate, 27, 3222–3247, https://doi.org/10.1175/ JCLI-D-13-00125.1.

Zhang, R., 2010: Latitudinal dependence of Atlantic meridional overturning circulation (AMOC) variations. Geophys. Res. Lett., 37, L16703, https://doi.org/10.1029/2010GL044474.